J. Iron Steel Res. Int. (2019) 26:374–384
https://doi.org/10.1007/s42243-019-00248-4

ORIGINAL PAPER

# Effect of $CaO/Al_2O_3$ ratio on viscosity and structure of $CaO–Al_2O_3$-based fluoride-free mould fluxes

Qi Wang[1] · Ji-an Yang[1] · Chen Zhang[2] · De-xiang Cai[2] · Jian-qiang Zhang[1] · Oleg Ostrovski[1]

Received: 14 October 2018 / Revised: 26 November 2018 / Accepted: 10 January 2019 / Published online: 19 March 2019


## Abstract

The effects of $CaO/Al_2O_3$ ratio on viscosity and structure of the $CaO-Al_2O_3$-based fluoride-free mould fluxes were investigated with the $CaO/Al_2O_3$ ratio varied from 1 to 4 and the content of $SiO_2$ fixed at 7 wt.%. The increase in the $CaO/Al_2O_3$ ratio from 1 to 2 lowered the viscosity of the flux melts. The viscosity increased slightly with the $CaO/Al_2O_3$ ratio from 2 to 3, and this increase became significant with further increasing $CaO/Al_2O_3$ ratio to 4. Both break temperature and apparent activation energy were found to be increased with the increase in $CaO/Al_2O_3$ ratio from 2 to 4. There was no break temperature available in the flux with $CaO/Al_2O_3$ ratio of 1. Changing the $CaO/Al_2O_3$ ratio from 1 to 2 decreased the apparent activation energy. Equilibrium phases of the fluxes were calculated using FactSage 7.1 and the major phases were found to be varied with the $CaO/Al_2O_3$ ratio. Structures of tested mould fluxes were analysed using Fourier transform infrared spectroscopy. The results showed that the increase in the $CaO/Al_2O_3$ ratio from 1 to 2 decreased the complexity of the structure, leading to a reduced viscosity. With the increase in the $CaO/Al_2O_3$ ratio from 2 to 4, both solid phase precipitation and melt structure contributed to the variation of viscosity.

**Keywords** $CaO–Al_2O_3$-based flux · $CaO/Al_2O_3$ ratio · Viscosity · Flux structure

## 1 Introduction

In steel production, continuous casting is a major operation. Mould fluxes play irreplaceable roles in the steel continuous casting, such as lubricating the stand, preventing steel from freezing, absorbing inclusions from molten steel, insulating steel from oxidation, and controlling heat transfer between the steel and mould [1–4]. Viscosity is one of the key properties of mould fluxes, which prominently affects the lubrication during casting, reaction kinetics, and diffusion in mould fluxes in high temperature region [5–7]. Temperature and composition are two major factors which affect the viscosity of mould fluxes.

High aluminium steel, such as transformation-induced plasticity (TRIP) steel, possesses outstanding mechanical properties and superior formability, making it attractive for application in the automotive industry [8]. However, in the process of continuous casting, [Al] in the steel reacts with $(SiO_2)$ in the conventional $CaO–SiO_2$-based mould fluxes, resulting in the reduction of $SiO_2$ and the oxidation of Al. Severe flux-metal reaction leads to changes of the flux chemical composition with a significant influence on the flux properties and causes reduction of the refining capacity of the flux and insufficient lubrication of flux with a detrimental effect on surface quality [9–12].

Studies on the modification of the $CaO–SiO_2$-based mould fluxes by optimizing the ratios of $CaO/SiO_2$ [13] as well as $Al_2O_3/SiO_2$ [14–16], and the amount of $Al_2O_3$ [17] showed that heat flux between steel and mould is unstable at the initial stage, and the experimental mould fluxes present a very strong crystallization tendency. Therefore, optimizing the conventional mould fluxes to restrict the flux-steel reaction is extremely hard. The fundamental way of solving the reaction problem is to develop a $CaO–Al_2O_3$-based mould flux system which partially suppresses the reaction between [Al] in the steel and $(SiO_2)$ in the mould flux [18]. Wang et al. [19] also proved that the CaO–

✉ Jian-qiang Zhang
j.q.zhang@unsw.edu.au

[1] School of Materials Science and Engineering, University of New South Wales, Sydney 2052, Australia

[2] Baosteel Group Corporation Research Institute, Shanghai 201900, China

$Al_2O_3$-based mould flux can markedly depress the flux-metal reaction and obviously enhance the slab surface quality. There are several studies [20–22] focusing on the application of $CaO–Al_2O_3$-based mould flux. However, most of them focused on the effects of other components, such as BaO [23–25], $Li_2O$ [13, 26, 27], $Na_2O$ [13, 28], MgO [23], and $B_2O_3$ [9], on mould flux performance, but few paid attentions to the effect of $CaO/Al_2O_3$ ratio. Therefore, it is essential to investigate the effect of $CaO/Al_2O_3$ ratio in a broad range on the viscosity and structure of lime alumina-based mould flux systematically.

Furthermore, it is known that $CaF_2$ is a volatile compound, causing health hazards, environmental pollution, and equipment corrosion [29, 30], which forces researchers using the substitute of fluoride, such as $B_2O_3$ [31–35] and $Na_2O$ [36, 37]. However, very few studies of fluoride-free $CaO–Al_2O_3$-based mould fluxes have been reported. Gao et al. [23] studied the effect of alkaline earth metal oxides on the viscosity and structure of $CaO–Al_2O_3$-based mould flux with a limited fluoride content (7 wt.%).

The aim of this study is to investigate the effect of $CaO/Al_2O_3$ ratio on the mould flux structure and viscosity and to provide further fundamental understanding of the effect of this parameter on flux properties which will be used for developing $CaO–Al_2O_3$ fluorine-free mould fluxes for high-Al steel casting.

## 2 Experimental

### 2.1 Experimental material preparation

The chemical compositions of samples used in this study are listed in Table 1. All these fluxes were prepared using analytical reagent grade chemicals $CaCO_3$, $SiO_2$, $Al_2O_3$, $B_2O_3$, $Na_2CO_3$, MgO, and $Li_2CO_3$. The well-mixed components were fully ground in an agate mortar for 20 min and then premelted in a high-purity graphite crucible at 1400 °C for 20 min. At high temperature, $CaCO_3$, $Na_2CO_3$, and $Li_2CO_3$ were decomposed, emitting $CO_2$ gas and forming CaO, $Na_2O$, and $Li_2O$, respectively. After that, the melt was water quenched and dried at 120 °C for 4 h and then ground into fine powders with an average size of 75 μm for the following experimental use. The $CaO/Al_2O_3$ weight ratio was fixed at 1, 2, 3, and 4, which covers a broad range of the $CaO/Al_2O_3$ ratios, allowing to reliably establish the effect of this ratio on the viscosity and the structure of the fluxes. The concentrations of $B_2O_3$ and $Li_2O$ were determined by inductive couple plasma (ICP), and other components were analysed by X-ray fluoroscopy (XRF). Due to the evaporation during melting process, weight losses of $B_2O_3$ and $Na_2O$ were observed; the measured concentrations of $B_2O_3$ and $Na_2O$ were below the designated values of 11 and 6 wt.%, respectively. The concentrations of $Na_2O$ in sample 1 and $B_2O_3$ in sample 4 were very close to the designated values.

**Table 1** Measured chemical composition of mould fluxes (wt.%)

| Sample | CaO | $Al_2O_3$ | C/A[a] | $SiO_2$ | $Na_2O$ | $B_2O_3$ | $Li_2O$ | MgO |
|---|---|---|---|---|---|---|---|---|
| 1 | 36.8 | 36.3 | 1 | 6.9 | 5.9 | 9.5 | 2.1 | 1.8 |
| 2 | 49.2 | 24.0 | 2 | 6.8 | 5.5 | 9.7 | 2.0 | 1.4 |
| 3 | 55.4 | 18.5 | 3 | 6.9 | 5.0 | 9.4 | 2.1 | 1.7 |
| 4 | 57.4 | 15.1 | 4 | 6.9 | 5.0 | 11.0 | 2.2 | 1.8 |

[a]*C/A* represents $CaO/Al_2O_3$ ratio

### 2.2 Viscosity measurement

Mould flux viscosity was measured using a rotating cylindrical viscometer (model ZC-1600, China). The schematic layout of the experimental set-up is given in Fig. 1. During the experiment, the Mo spindle (diameter: 15 mm; height: 30 mm) was rotating at a fix speed of 12 r/min; a Pt/Rh thermocouple (B-type) was placed right beneath the bottom of a high-purity graphite crucible (inner diameter: 40 mm; inner height: 160 mm). Protective nitrogen gas was employed to prevent the oxidation of a graphite crucible and a molybdenum spindle. In every measurement, 140 g flux sample was placed in the crucible, heated to 1400 °C, and held for 20 min to obtain a homogeneous melt. The temperature of the furnace was controlled within ± 2 °C. It decreased with a rate of 5 °C/min, and the viscosity of experimental flux was continuously recorded. The experimental set-up and procedure were presented in detail elsewhere [38].

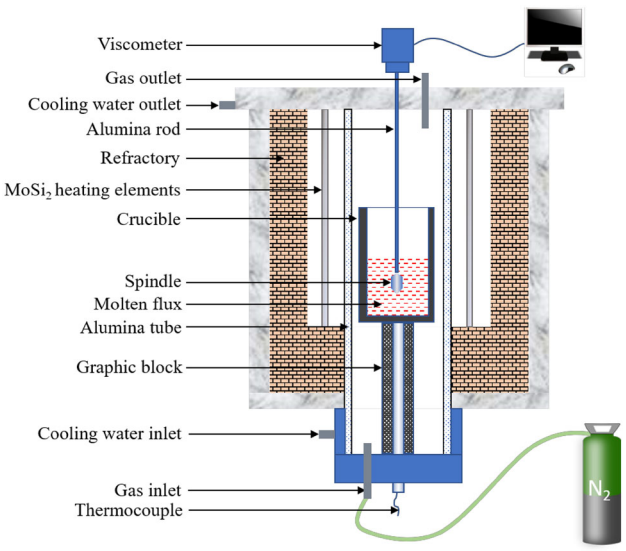


**Fig. 1** Schematic diagram of viscometer for viscosity measurement

### 2.3 Fourier transform infrared spectroscopy

The effect of $CaO/Al_2O_3$ ratio on the structure of mould fluxes was studied using a Fourier transform infrared spectrometer (FTIR, Spotlight 400; PerkinElmer, USA). The as-quenched samples were ground into fine powders with the average size of 100 μm. For FTIR testing, 2.0 mg sample powder and 200 mg KBr were well mixed in an agate mortar and pressed into a cylindrical pellet. FTIR-transmitting spectra with a KBr detector were taken in the range of 4000 to 450 $cm^{-1}$ with a resolution of 2 $cm^{-1}$. The FTIR transmission spectra of studied samples were mainly focused in the range of 1600 to 400 $cm^{-1}$ [39–41].

## 3 Results and discussion

### 3.1 Effect of $CaO/Al_2O_3$ ratio on flux viscosity

The results of viscosity measurements are plotted in Fig. 2 (where $\eta$ is the viscosity of mould flux, Pa s). The starting measurement temperature for all fluxes was 1400 °C. During continuous cooling process, when the flux was in the liquid state, the viscosity was low. With the decrease in temperature, the viscosity increased gradually. For samples 1–3 with low $CaO/Al_2O_3$ ratios, the viscosity of liquid flux was in the range of 0.12 to 0.60 Pa s, while for sample 4, the viscosity range increased to 1.2–1.5 Pa s. When the temperature dropped to a certain value, the viscosity increased sharply, which corresponds to the break temperature ($T_{br}$). At this temperature, a large number of bulk crystals appeared and formed a solid–liquid state [42–44].

For sample 1 with $CaO/Al_2O_3$ of 1, the viscosity increased gradually in the cooling process and no sharp change in viscosity was observed, and thus, no corresponding $T_{br}$ was found. Viscosity curves of mould fluxes with $CaO/Al_2O_3$ ratios of 2 and 3 had a similar profile (Fig. 2b, c) where viscosity increased sharply when the break temperature was reached. Viscosity of sample 4 with $CaO/Al_2O_3$ of 4 (Fig. 2d) increased with different rates in different temperature ranges. The break temperatures of fluxes $T_{br}$ are listed in Table 2.

Figure 3 shows the viscosity of the mould fluxes as a function of $CaO/Al_2O_3$ ratio in the temperature range from 1325 to 1400 °C. The viscosity of flux with $CaO/Al_2O_3$ ratio of 4 at 1325 °C is not shown as this temperature is below the break temperature. It can be seen from Fig. 3 that the viscosity of the melt decreased with the increasing $CaO/Al_2O_3$ ratio from 1 to 2. A slight rise in the viscosity was observed when the $CaO/Al_2O_3$ ratio increased from 2 to 3. A significant rise in viscosity occurred with a further increase in the $CaO/Al_2O_3$ ratio from 3 to 4. In general, reducing temperature increased the viscosity.

### 3.2 Activation energy and break temperature

Liquid flux can be assumed to be a Newtonian fluid when temperature is above the break temperature. The change in the viscosity with temperature follows the Arrhenius equation:

$$\eta = A\exp\left(\frac{E_a}{RT}\right) \tag{1}$$

where $T$ stands for the absolute temperature, K; $A$ is a constant; $E_a$ represents the apparent activation energy for viscous flow, kJ $mol^{-1}$; and $R$ is the ideal gas constant which equals to 8.314 J $mol^{-1}$ $K^{-1}$. The activation energy can be found using Eq. (2).

$$\ln\eta = \frac{E_a}{RT} + \ln A \tag{2}$$

The plot of $\ln\eta$ versus $1/T$ is shown in Fig. 4 with an excellent linear fitting for all samples (coefficient of determination $R^2 \geq 0.95$ in Table 2), and the activation energy (with $R^2$ values) is listed in Table 2. As mentioned before, $T_{br}$ was not obtained for flux with $CaO/Al_2O_3$ of 1. The apparent activation energy for this flux was found to be 175 kJ $mol^{-1}$. The apparent activation energy increased from 168 to 180 kJ $mol^{-1}$ with the increase in $CaO/Al_2O_3$ ratio from 2 to 4.

Table 2 also presents the calculated liquidus temperatures ($T_{liq}$) and calculated solidus temperatures ($T_{sol}$) of fluxes with different $CaO/Al_2O_3$ ratios obtained using thermochemical software FactSage 7.1.

The $T_{liq}$ of sample 4 with $CaO/Al_2O_3$ of 4 was extremely high (above 1500 °C), compared with those of the other three samples. However, the $T_{sol}$ of sample 4 showed the lowest value (793 °C). With increasing $CaO/Al_2O_3$ ratio from 1 to 2, the $T_{sol}$ increased from 842 to 879 °C; with further increasing $CaO/Al_2O_3$ ratio to 3, the $T_{sol}$ decreased from 879 to 793 °C; and sample 3 ($CaO/Al_2O_3$ = 3) and sample 4 ($CaO/Al_2O_3$ = 4) had the same $T_{sol}$ value.

### 3.3 Calculated phase composition

The equilibrium phases of the experimental mould fluxes calculated using thermochemical software FactSage 7.1 are shown in Fig. 5. The phase equilibrium calculation revealed that, when $CaO/Al_2O_3$ ratio was 1 (Fig. 5a), the dominant phases were $Na_2CaAl_4O_8$ and $Mg_3B_2O_6$. With the increase in $CaO/Al_2O_3$ ratio from 1 to 2 (Fig. 5a, b), phase $Ca_{11}B_2Si_4O_{22}$ became significant and $Mg_3B_2O_6$ disappeared; $Na_2CaAl_4O_8$ still existed but tended to be less

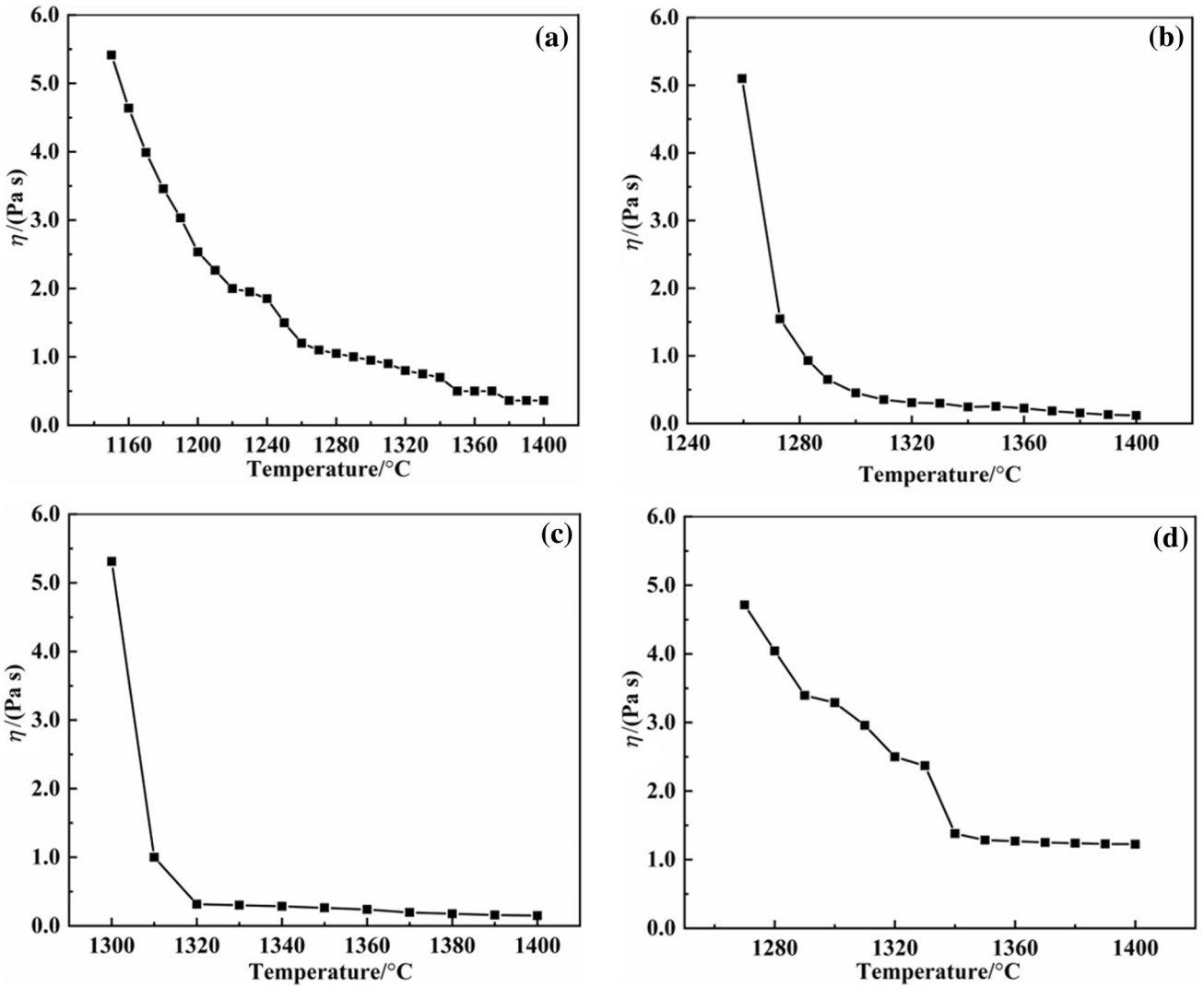


**Fig. 2** Effect of $CaO/Al_2O_3$ ratio on viscosity. **a** $CaO/Al_2O_3$ = 1; **b** $CaO/Al_2O_3$ = 2; **c** $CaO/Al_2O_3$ = 3; **d** $CaO/Al_2O_3$ = 4

**Table 2** Calculated $E_a$, $T_{br}$, $T_{liq}$, and $T_{sol}$ for fluxes with different $CaO/Al_2O_3$ ratios

| $CaO/Al_2O_3$ ratio | $E_a$/(kJ mol$^{-1}$) | $R^2$ | $T_{br}$/°C | $T_{liq}$/°C | $T_{sol}$/°C |
|---|---|---|---|---|---|
| 1 | 175 | 0.946 | – | 1232 | 842 |
| 2 | 168 | 0.989 | 1289 | 1277 | 879 |
| 3 | 170 | 0.976 | 1320 | 1387 | 793 |
| 4 | 180 | 0.996 | 1338 | > 1500 | 793 |

noticeable; $Ca_2SiO_4$, however, appeared and became the main crystal phase at the high temperature.

With further increasing $CaO/Al_2O_3$ ratio from 2 to 3 (Fig. 5b, c), the region of $Ca_2SiO_4$ became larger in the high temperature region. CaO also became an apparent high-temperature phase. The area of $Ca_{11}B_2Si_4O_{22}$ decreased a bit; the area of $Na_2CaAl_4O_8$ trended to shrink and existed in the relatively low-temperature zone. With further increase in $CaO/Al_2O_3$ ratio from 3 to 4 (Fig. 5c, d), CaO phase became more pronounced, and $Ca_2SiO_4$ was partially substituted by CaO; the regions of both $Ca_{11}B_2Si_4O_{22}$ and $Na_2CaAl_4O_8$ remained less prominent.

### 3.4 FTIR spectroscopy

Results of FTIR analysis of as-quenched mould fluxes with varying $CaO/Al_2O_3$ ratio are shown in Fig. 6. Three wave number regions can be distinguished in the FTIR spectra, 450–800, 800–1100, and 1100–1600 cm$^{-1}$. Detailed assignment of FTIR band groups corresponding to different wave number regions is presented in Table 3. The reflection peak located at 500–600 cm$^{-1}$ represents the

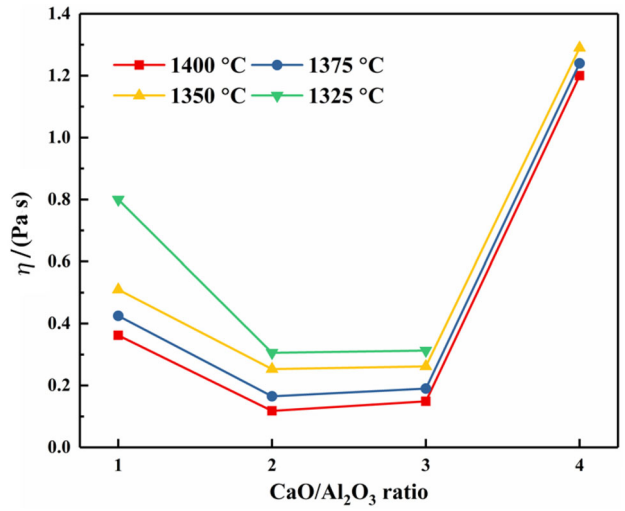


**Fig. 3** Viscosity of mould fluxes versus $CaO/Al_2O_3$ ratio at different temperatures

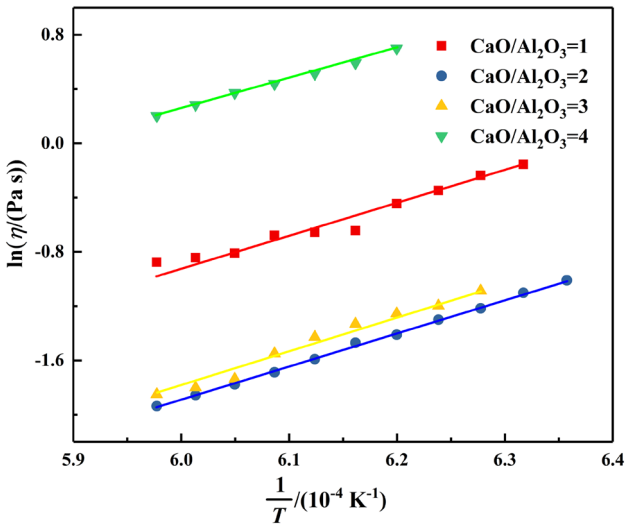


**Fig. 4** Plots of $\ln\eta$ versus $T^{-1}$ for fluxes with $CaO/Al_2O_3$ ratio from 1 to 4

asymmetric stretching vibration of $[AlO_6]$-octahedron [27]; the transmittance spectrum around 650 $cm^{-1}$ is assigned to the symmetric stretching vibration of $[AlO_4]$-tetrahedral [9]; the transmittance curve placed at 800–1200 $cm^{-1}$ corresponds to the $[SiO_4]$-tetrahedral structural units region [45]; and bands at around 1250, 1350, and 1450 $cm^{-1}$ were assigned to B–O stretching vibration of varied borate groups in $[BO_2O^-]$, B–O stretching vibration of varied borate groups in $[BO_3]$ units, and B–O stretching vibration of $[BO_3]$ in boroxol rings [46], respectively.

Aluminium ion in the flux structure occupied both tetrahedral and octahedral positions, which reflects an amphoteric nature of aluminium oxide. With increasing $CaO/Al_2O_3$ ratio, the transmittance trough of $[AlO_6]$-octahedron at 500–600 $cm^{-1}$ was first gradually deepened ($CaO/Al_2O_3$ ratio from 1 to 2), then remained constant ($CaO/Al_2O_3$ ratio from 2 to 3), and finally became shallower ($CaO/Al_2O_3$ ratio from 3 to 4), indicating the complex structure of mould flux [27]. With the increase in $CaO/Al_2O_3$ ratio, the transmittance trough of symmetric stretching vibration of $[AlO_4]$-tetrahedral at about 650 $cm^{-1}$ shifted towards lower wave number region and the width of the band tended to become narrower, which suggested a decrease in the degree of polymerization (DOP) as $Al_2O_3$ exhibited property of a network-forming oxide. Similar results were obtained by Yan et al. [47] in their study of the effect of $CaO/Al_2O_3$ ratio on structure of $CaO–Al_2O_3–20\%$ $CaF_2–10\%$ $B_2O_3–10\%$ $Na_2O–5\%$ $SiO_2$ system.

In the silicate structures, increasing $CaO/Al_2O_3$ ratio from 1 to 2 moved the band to the left towards lower wave number and the band width of the silicate region became narrower. Further increasing $CaO/Al_2O_3$ ratio from 2 to 4 made no noticeable band shift and width change. The increase in $CaO/Al_2O_3$ ratio also had a minor effect on the borate structure in the region of 1100–1600 $cm^{-1}$.

For quantitative analyses of the structural units, absorbance–wave number curves of FTIR spectra should be employed, as the area of the structural unit in the absorbance–wave number curve is in proportion to its concentration in the sample, which is invalid in the corresponding transmittance–wave number curve [48]. FTIR spectra of mould fluxes can be converted into absorbance–wave number curves from the original transmittance–wave number curves by using the Beer law [49].

$$T' = I/I_0 \times 100\% \tag{3}$$

$$A' = \lg(I_0/I) \times 100\% \tag{4}$$

where $T'$ and $A'$ are light transmittance and absorbance; $I$ is the transmitted light intensity; and $I_0$ is the initial light intensity. The absorbance–wave number profiles can be obtained from the original transmittance–wave number ones using Eq. (5):

$$A' = \lg(1/T') \tag{5}$$

The absorbance curves for fluxes with varied $CaO/Al_2O_3$ ratios are presented in Fig. 7 for the wave number between 450 and 1100 $cm^{-1}$. IR spectra (infrared spectra) were fitted using the Gaussian deconvolution method as shown also in Fig. 7. The band around 400–500 $cm^{-1}$ is related to the deformation of tetrahedron and octahedron units [50]. The band around 550 $cm^{-1}$ is assigned to the Al–O–Al bond bending vibrations [51]. According to Kamitsos et al. [46], characteristic band at around 760 $cm^{-1}$ reflects the B–O–B bond bending vibrations in

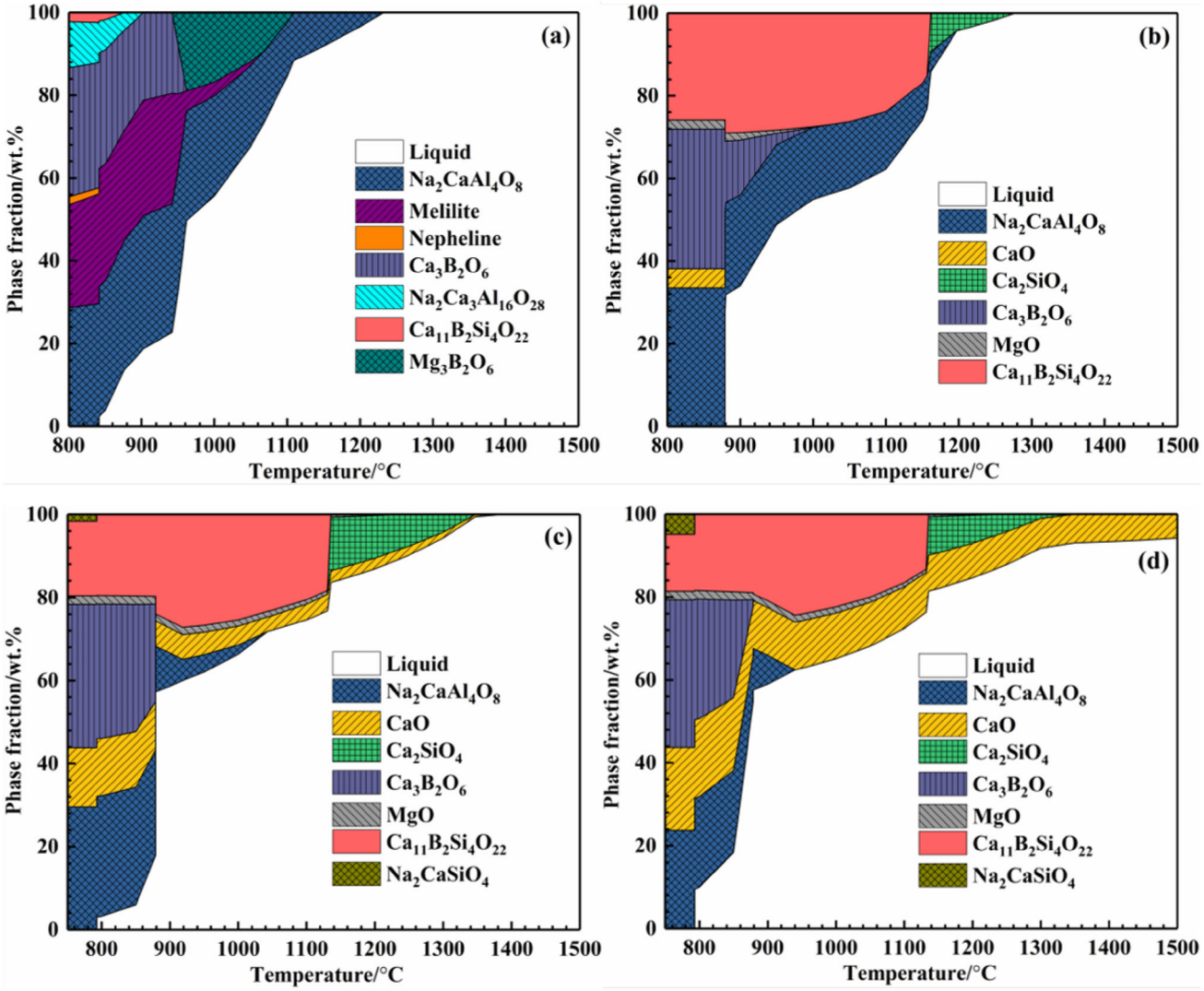


**Fig. 5** Calculated equilibrium phases of samples with varying $CaO/Al_2O_3$ ratios using FactSage 7.1. **a** $CaO/Al_2O_3 = 1$; **b** $CaO/Al_2O_3 = 2$; **c** $CaO/Al_2O_3 = 3$; **d** $CaO/Al_2O_3 = 4$

pentaborate and band at around 900 $cm^{-1}$ represents the B–O asymmetric stretching vibrations of $[BO_4]$-tetrahedral. The band in the range of 780–800 $cm^{-1}$ was assigned to the Si–O-Si bending vibration [52]. The characteristic peaks located at 840–870, 920–930, 970–1000, 1050–1075, and 1100–1150 $cm^{-1}$ were assigned to the $Si–O^-$ symmetric stretching of various structural units, containing $SiO_4^{4-}$ monomers, $Si_2O_7^{6-}$ dimers, $SiO_3^{2-}$ chains or rings, $Si_2O_5^{2-}$ sheets, and $SiO_2$ three-dimensional units [52, 53]. The IR spectra are used to estimate fractions of bridging and non-bridging oxygen in different structural units, which are characterized by $Q^n$, where $n$ is a number of bridging oxygens per silicon ion: $Q^0$ (NBO/Si = 4), $Q^1$ (NBO/Si = 3), $Q^2$ (NBO/Si = 2), $Q^3$ (NBO/Si = 1), and $Q^4$ (NBO/Si = 0).

## 4 Discussion

As shown above, $CaO/Al_2O_3$ ratio affects viscosity, equilibrium phases, and structures of mould fluxes. Above the break temperature, the viscosity of the melt decreased with increasing the $CaO/Al_2O_3$ ratio from 1 to 2. With increasing the $CaO/Al_2O_3$ ratio from 2 to 3, there was a slight rise of the viscosity. The viscosity increased significantly when the $CaO/Al_2O_3$ ratio increased from 3 to 4. The break temperature and activation energy were found to increase with the increase in $CaO/Al_2O_3$ ratio from 2 to 4, while for sample 2, the activation energy was lower than that for sample 1 (Table 2). This observation is generally considered to be related to varied phase formation and flux structure at different temperatures during cooling process as discussed below.

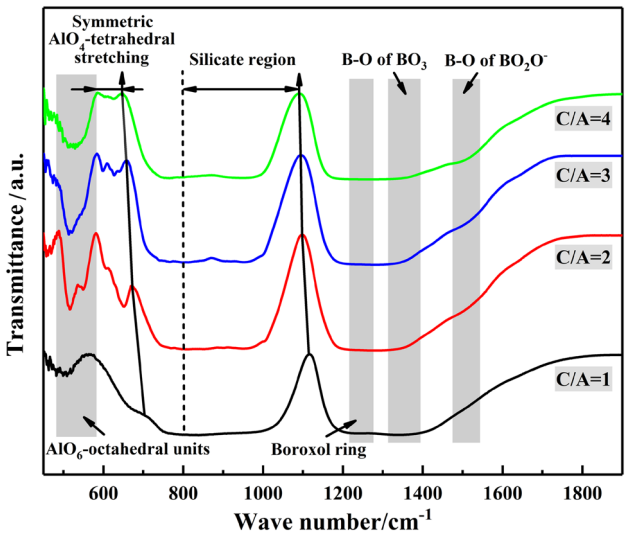


**Fig. 6** FTIR spectra of as-quenched samples with various $CaO/Al_2O_3$ ratios

**Table 3** Assignments of FTIR bands

| Wave number/ $cm^{-1}$ | Assignment | Ref. |
|---|---|---|
| 400–500 | Deformation of tetrahedron and octahedron units | [51] |
| 500–600 | Asymmetric stretching vibration of $[AlO_6]$-octahedron | [27] |
| ~ 550 | Al–O–Al bond bending vibrations | [9] |
| ~ 650 | Symmetric stretching vibration of $[AlO_4]$-tetrahedral | [9] |
| ~ 760 | B–O–B bond bending vibrations from pentaborate | [46] |
| 780–800 | Si–O–Si bond bending vibrations | [52] |
| 840–870 | Symmetric stretching Si–$O^-$ of $[SiO_4]^{4-}$ ($Q_0$ or NBO/Si = 4) | [52, 53] |
| 920–930 | Symmetric stretching Si–$O^-$ of $[Si_2O_7]^{6-}$ ($Q_1$ or NBO/Si = 3) | [52, 53] |
| 970–1000 | Symmetric stretching Si–$O^-$ of $[SiO_3]^{2-}$ ($Q_2$ or NBO/Si = 2) | [52, 53] |
| 1050–1075 | Symmetric stretching Si–$O^-$ of $[Si_2O_5]^{2-}$ ($Q_3$ or NBO/Si = 1) | [52, 53] |
| 800–1200 | B–O bond in $[BO_4]$-tetrahedral units | [46] |
| ~ 1250 | B–O stretching vibration of $[BO_3]$ in boroxol rings | [46] |
| ~ 1350 | B–O stretching vibration of varied borate groups in $[BO_2O^-]$ | [46] |
| ~ 1450 | B–O stretching vibration of varied borate groups in $[BO_3]$ units | [46] |

## 4.1 Effect of $CaO/Al_2O_3$ ratio on flux structure

According to the deconvolution of IR spectra for quenched fluxes with different $CaO/Al_2O_3$ ratios (Fig. 7), area fractions ($f$) of different characteristic peaks referred to total area in the whole measured wave number range are listed in Table 4. The relative area percentages of various silicate structural units in reference to total silicates are shown in Fig. 8, and area fractions of aluminate unit structures are shown in Fig. 9.

For silicate units, in fluxes with $CaO/Al_2O_3$ ratio from 1 to 3, $Q^0$ was the dominant unit, while among samples with $CaO/Al_2O_3$ ratio of 2, 3, and 4, $Q^3$ was not distinguishable in the IR spectra. No $Q^4$ was detected for all fluxes. Area fractions of $Q^0$, $Q^2$, and $Q^3$ decreased, while that of $Q^1$ increased significantly from 12% to 37% with increasing $CaO/Al_2O_3$ ratio from 1 to 2. With increasing $CaO/Al_2O_3$ ratio from 2 to 3, the relative area fractions of silicate groups varied in an opposite direction; the relative fraction of $Q^1$ sharply decreased from 37% to 3%, while that of both $Q^0$ and $Q^2$ increased, especially for $Q^2$ raising from 11% to 34%. With further increase in $CaO/Al_2O_3$ ratio from 3 to 4, $Q^2$ became the dominant unit, while $Q^1$ disappeared. The degree of depolymerization of silicate group can be evaluated by non-bridging oxygen per silicon (NBO/Si) of the silicate group which can be estimated from the following equation [53] by using relative silicate unit fractions in Fig. 8:

$$\mathrm{NBO/Si} = \sum_{n=1}^{4} n \times \left(F_{Q^{4-n}}\right) \tag{6}$$

where $F_{Q^{4-n}}$ is the peak area fraction of $Q^{4-n}$ structure unit in total area of silicate units.

The values of NBO/Si are shown in Fig. 8 (also listed in Table 4) which indicate that with increasing the $CaO/Al_2O_3$ ratio from 1 to 4, NBO/Si decreased slightly for $CaO/Al_2O_3$ ratio from 1 to 3 but significantly for $CaO/Al_2O_3$ ratio from 3 to 4. The decrease in NBO/Si indicates an increase in the degree of polymerization of silicate group.

The effect of aluminate group becomes important because of high alumina concentration compared with the conventional silica-based flux. In the aluminate structure, the area fraction of $[AlO_6]$-octahedron increased, while that of $[AlO_4]$-tetrahedron decreased with the increase in $CaO/Al_2O_3$ ratio from 1 to 3, and the tendency of fraction variation for both aluminate structures was stable with the further increase in $CaO/Al_2O_3$ ratio to 4.

McMillan and Piriou [54] suggested that continually adding CaO into the aluminates instigated the weakening of the network of tetrahedral aluminate units and the formation of octahedral aluminate units with higher average coordination linkage for accommodating the redundant oxygen.

$$[AlO_4]^{5-} + 2O^{2-} = [AlO_6]^{9-} \tag{7}$$

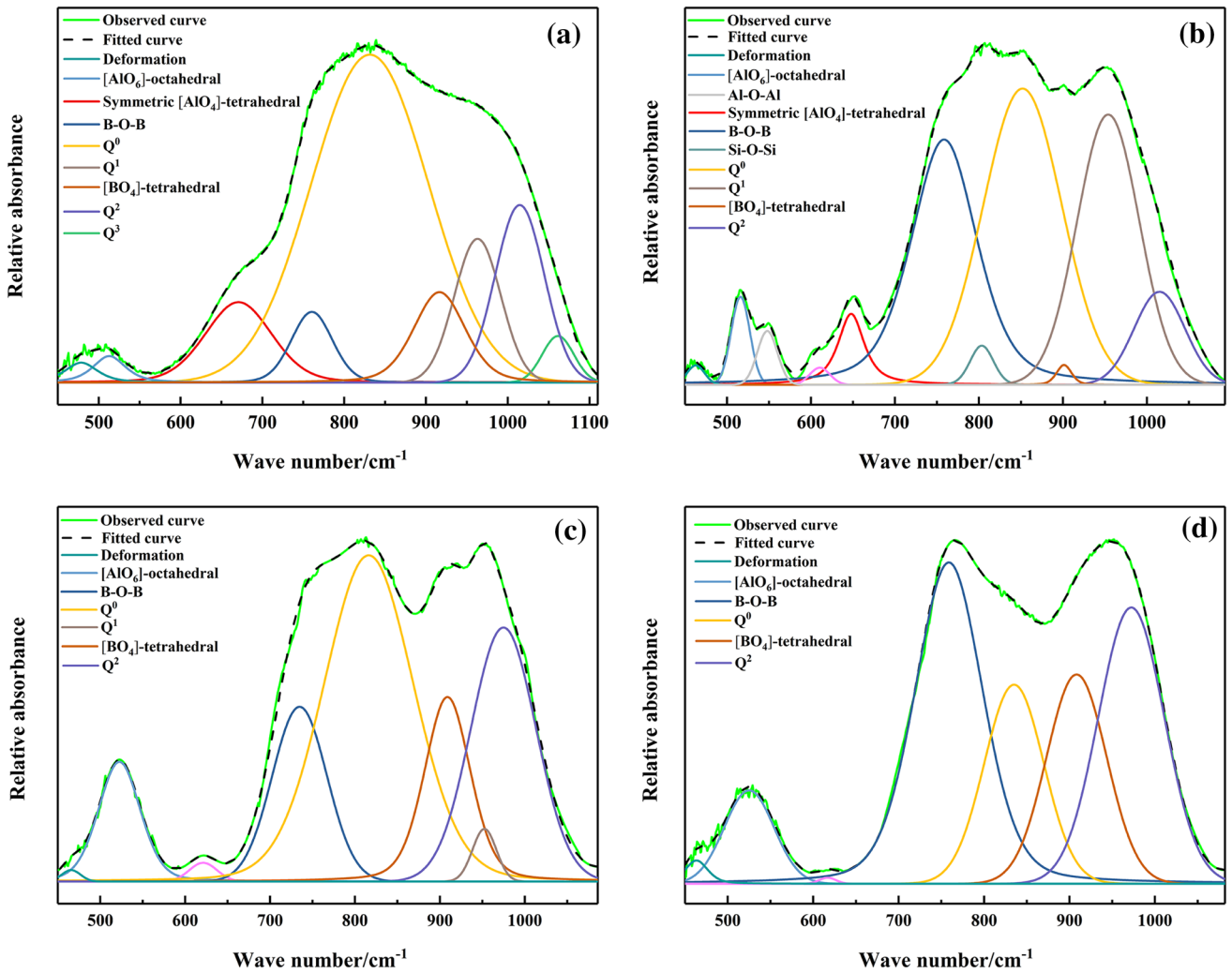


**Fig. 7** Deconvolution of IR spectra for quenched fluxes with different $CaO/Al_2O_3$ ratios. **a** $CaO/Al_2O_3$ = 1; **b** $CaO/Al_2O_3$ = 2; **c** $CaO/Al_2O_3$ = 3; **d** $CaO/Al_2O_3$ = 4

**Table 4** Area fractions of different structural units for mould fluxes with various $CaO/Al_2O_3$ ratios

| $CaO/Al_2O_3$ ratio | $f_{Q^0}$ | $f_{Q^1}$ | $f_{Q^2}$ | $f_{Q^3}$ | $f_{AlO_6}$ | $f_{AlO_4}$ | $f_{(BO_4)}$ | $f_{(B-O-B)}$ | NBO/Si |
|---|---|---|---|---|---|---|---|---|---|
| 1 | 0.282 | 0.049 | 0.064 | 0.011 | 0.008 | 0.043 | 0.039 | 0.023 | 3.47 |
| 2 | 0.168 | 0.121 | 0.034 | | 0.012 | 0.018 | 0.003 | 0.137 | 3.41 |
| 3 | 0.204 | 0.008 | 0.109 | | 0.037 | | 0.063 | 0.063 | 3.29 |
| 4 | 0.074 | | 0.151 | | 0.034 | | 0.078 | 0.150 | 2.66 |

The area fraction of $[AlO_6]$-octahedron increased, while that of $[AlO_4]$-tetrahedron decreased with the increase in $CaO/Al_2O_3$ ratio from 1 to 3, indicating the reforming of the network structure. After $CaO/Al_2O_3$ ratio exceeding 3, the area fractions of both $[AlO_6]$-octahedra and $[AlO_4]$-tetrahedra tend to be flat because no more $[AlO_4]$-tetrahedra left.

For borate units, only $[BO_4]$-tetrahedral and B–O–B pentaborate were quantitatively analysed. Therefore, no relative area fractions of these units referred to total borate units were given, as for silicate and aluminate cases in Figs. 8 and 9. According to Table 4, the area fraction of $[BO_4]$-tetrahedral structural units first descended with increasing $CaO/Al_2O_3$ ratio from 1 to 2 and then

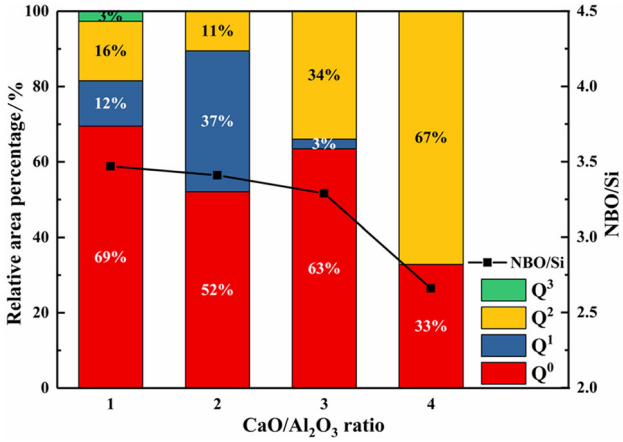


**Fig. 8** Relative area percentages of silicate structural units for mould fluxes with different $CaO/Al_2O_3$ ratios and non-bridging oxygen per silicon (NBO/Si) of silicate group

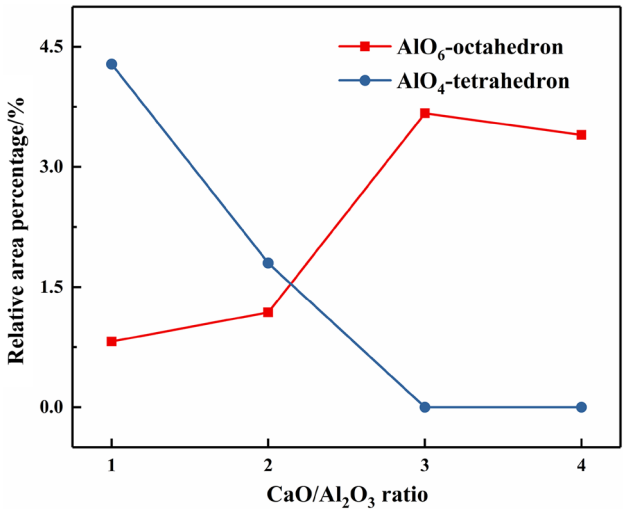


**Fig. 9** Relative area percentages of aluminate unit structures for mould fluxes with different $CaO/Al_2O_3$ ratios

continuously increased with further increase in $CaO/Al_2O_3$ ratio to 4. For B–O–B bending vibrations from pentaborate, the area fraction of boroxol ring structure [35] first increased with increasing the $CaO/Al_2O_3$ ratio from 1 to 2 and then decreased with increasing $CaO/Al_2O_3$ ratio to 3, but finally increased with further increasing $CaO/Al_2O_3$ ratio to 4. The variation of B–O–B bending vibrations with $CaO/Al_2O_3$ ratio is in an opposite direction with that of $[BO_4]$-tetrahedral structural units in the same $CaO/Al_2O_3$ ratio range of 1 to 3. The reason for the variation in both areas of B–O–B bending vibrations and $[BO_4]$-tetrahedral structural units could be explained by the transformation between varied borate units, which is affected by the contents of other components, e.g. CaO and $Al_2O_3$. According to Klyuev and Pevzner [55], the transformation between $[BO_3]$-triangular structural units and $[BO_4]$-tetrahedral structural units depends on CaO content. When CaO content is higher than 40 mol% which is the case for all fluxes investigated, $[BO_3]$-triangular structural units are produced at the expense of $[BO_4]$-tetrahedral structural units, thus reforming the structure [55]. With the increase in $CaO/Al_2O_3$ ratio, the relative content of $Al_2O_3$ decreased, and as a result, $[BO_4]$-tetrahedral structural units were formed which increased the degree of flux polymerization [9]. Therefore, there is a balance between the decrease in $[BO_4]$-tetrahedral structural units caused by CaO content increase and the increase in $[BO_4]$-tetrahedral structural units caused by $Al_2O_3$ decrease.

## 4.2 Effect of $CaO/Al_2O_3$ ratio on viscosity

It is well known that flux viscosity is related to the melt structure. For $CaO–Al_2O_3$-based fluxes, aluminate structure becomes dominant. The FTIR structural analysis revealed that increasing $CaO/Al_2O_3$ ratio from 1 to 3 leads to an increase in the fraction of $[AlO_6]$-octahedron but an decrease in the fraction of $[AlO_4]$-tetrahedron. This structural change can be correlated to the decrease in the structural complexity, and therefore, from this aspect, the viscosity should be decreased. This is in fact true for the $CaO/Al_2O_3$ ratio from 1 to 2 as shown in Fig. 3. Furthermore, the decrease in the fraction of $[BO_4]$-tetrahedral structural unit with the increasing $CaO/Al_2O_3$ ratio from 1 to 2 could also lead to the reduction in viscosity due to the reduced amount of polymerized borate structure. For the silicate units, the NBO/Si determined in Table 4 as well as Fig. 8 showed no significant change when $CaO/Al_2O_3$ ratio increased from 1 to 2, suggesting the minor effect of silicate structural units on the DOP of these mould fluxes. Therefore, the decrease in viscosity for the $CaO/Al_2O_3$ ratio from 1 to 2 is attributed to the decrease in structural complexity of aluminates and borates.

With further increasing $CaO/Al_2O_3$ ratio from 2 to 3, the fractions of aluminate structures changed in a similar manner as those for 1 to 2, but the fraction of $[BO_4]$-tetrahedral structure showed an opposite trend. For silicate group, with further increasing $CaO/Al_2O_3$ ratio to 3, the NBO/Si had a slight decrease. It is known that viscosity was affected by both the flux structure and the precipitation of the solid phase. Based on Sect. 3.3, the liquidus temperature of mould flux increased with the increasing $CaO/Al_2O_3$ ratio; especially for the range of 2 to 4, high-temperature phases such as $Ca_2SiO_4$ and CaO (Fig. 5) appeared. The comprehensive effect of melt structure and precipitation of the solid phase could result in no obvious change in viscosity for mould flux with $CaO/Al_2O_3$ ratio increasing from 2 to 3.

With further increasing $CaO/Al_2O_3$ ratio from 3 to 4, both the area fraction of $[BO_4]$-tetrahedral structure and

aluminate structures exhibited no significant change, while a noticeable decrease was observed in NBO/Si of silicate group. The calculated liquidus temperature of mould flux for Flux 4 is above 1500 °C, making the flux heterogeneous in the temperature range of viscosity measurements. By this consideration, a sharp rise in the flux viscosity when the $CaO/Al_2O_3$ ratio increases from 3 to 4 should be attributed to the increase in liquidus temperature of sample 4.

### 4.3 Effect of $CaO/Al_2O_3$ ratio on precipitation of crystal phases and its correlation with break temperature

The value of $T_{br}$ increased from 1289 to 1338 °C with increased $CaO/Al_2O_3$ ratio from 2 to 4. $T_{br}$ is attributed to the formation of solid substances in the melts, and therefore, it can correlate with the liquidus temperature of the flux. Equilibrium phase calculations showed that this temperature increased with the increase in $CaO/Al_2O_3$ ratio which is, in principle, consistent with the trend in the change of $T_{br}$. For the flux with $CaO/Al_2O_3$ ratio of 2, $T_{br}$ was slightly higher than $T_{liq}$. Such imbalance between $T_{br}$ and $T_{liq}$ can be related to the experimental error in the measurement of $T_{br}$ (± 10 °C), and some change in the flux composition due to vaporization of $Na_2O$ and $B_2O_3$ [38], which could lead to the increase in $T_{liq}$, and these factors were not considered in the calculation of $T_{liq}$. The calculated $T_{liq}$ increased significantly when $CaO/Al_2O_3$ ratio increases to 3 and 4, while $T_{br}$ increased only by 18 °C. It follows from the phase composition in Fig. 5 that the increase in the liquidus temperature was caused by CaO precipitation, which started at $CaO/Al_2O_3$ ratio of 3 (Fig. 5c) and became significant at $CaO/Al_2O_3$ ratio of 4 (Fig. 5d). Precipitation of CaO could increase viscosity although the increase was not sharp. It should also be mentioned that the system was not in the equilibrium state in the process of cooling.

## 5 Conclusions

1. The viscosity of the flux melts decreased with an increase in the $CaO/Al_2O_3$ ratio from 1 to 2. From $CaO/Al_2O_3$ ratio = 2 to $CaO/Al_2O_3$ ratio = 3, there was a slight rise of the viscosity. The viscosity increased significantly when the $CaO/Al_2O_3$ ratio increased from 3 to 4.
2. FTIR results showed that the flux structure changed with changing $CaO/Al_2O_3$ ratio. With the increase in $CaO/Al_2O_3$ ratio from 1 to 2, the melt structure was controlled by the aluminate and borate group units; as a result, the structure complexity was decreased, leading to a reduced viscosity. With the increase in $CaO/Al_2O_3$ ratio from 2 to 4, both solid phase precipitation and melt structure contributed to the variation of viscosity.
3. With the increasing $CaO/Al_2O_3$ ratio, the apparent activation energy first decreased from 175 to 168 kJ $mol^{-1}$ and then increased from 168 to 180 kJ $mol^{-1}$, which is in the same trend as viscosity. The value of $T_{br}$ increased from 1289 to 1338 °C with the increase in $CaO/Al_2O_3$ ratio from 2 to 4.

**Acknowledgements** Financial supports from Baosteel-Australia Joint Research and Development Centre (BAJC) and Australian Research Council (ARC) Industrial Transformation Hub are greatly acknowledged. The first author also acknowledges the scholarship support from UNSW Australia (Tuition Fee Scholarship) and the China Scholarship Council (CSC Award).

## References

[1] L.J. Zhou, W.L. Wang, F.J. Ma, J. Li, J. Wei, H. Matsuura, F. Tsukihashi, Metall. Mater. Trans. B 43 (2012) 354–362.
[2] K.C. Mills, A.B. Fox, Z. Li, R.P. Thackray, Ironmak. Steelmak. 32 (2005) 26–34.
[3] W.L. Wang, A.W. Cramb, ISIJ Int. 45 (2005) 1864–1870.
[4] A. Yamauchi, K. Sorimachi, T. Sakuraya, T. Fujii, ISIJ Int. 33 (1993) 140–147.
[5] J. Jia, C. Bai, G. Qiu, D. Chen, Y. Xu, VII International Conference on Molten Slags, Fluxes and Salts, Johannesburg, South Africa, 2004, pp. 137–139.
[6] I. Sohn, D.J. Min, Steel Res. Int. 83 (2012) 611–630.
[7] S.F. Zhang, X. Zhang, W. Liu, X.W. Lv, C.G. Bai, L. Wang, J. Non-Cryst. Solids 402 (2014) 214–222.
[8] O. Grassel, L. Kruger, G. Frommeyer, L.W. Meyer, Int. J. Plast. 16 (2000) 1391–1409.
[9] G.H. Kim, I. Sohn, Metall. Mater. Trans. B 45 (2014) 86–95.
[10] W.L. Wang, Z.C. Luo, H.H. Zhang, Metall. Mater. Trans. B 49 (2018) 1034–1045.
[11] M. Lenoir, A. Grandjean, Y. Linard, B. Cochain, D.R. Neuville, Chem. Geol. 256 (2008) 316–325.
[12] G.H. Kim, I. Sohn, J. Non-Cryst. Solids 358 (2012) 1530–1537.
[13] B. Lu, K. Chen, W. Wang, B. Jiang, Metall. Mater. Trans. B 45 (2014) 1496–1509.
[14] J. Liao, Y. Zhang, S. Sridhar, X. Wang, Z. Zhang, ISIJ Int. 52 (2012) 753–758.
[15] Z. Zhang, G.H. Wen, P. Tang, S. Sridhar, ISIJ Int. 48 (2008) 739–746.
[16] Z. Zhang, G. Wen, J. Liao, S. Sridhar, Steel Res. Int. 81 (2010) 516–528.
[17] H.G. Ryu, Z.T. Zhang, J.W. Cho, G.H. Wen, S. Sridhar, ISIJ Int. 50 (2010) 1142–1150.
[18] D.L. Zheng, C.B. Shi, Z.J. Li, J. Li, J.W. Cho, J. Iron Steel Res. Int. (Revised version appears online on 2019-01-04). https://doi.org/10.1007/s42243-018-0218-9.
[19] W. Wang, B. Lu, D. Xiao, Metall. Mater. Trans. B. 47 (2016) 384–389.
[20] K. Blazek, H.B. Yin, G. Skoczylas, M. McClymonds, M. Frazee, AIST Trans. 8 (2011) 232–240.
[21] J.W. Cho, K. Blazek, M. Frazee, H.B. Yin, J.H. Park, S.W. Moon, ISIJ Int. 53 (2013) 62–70.

[22] C.B. Shi, M.D. Seo, J.W. Cho, S.H. Kim, Metall. Mater. Trans. B 45 (2014) 1081–1097.
[23] E.Z. Gao, W.L. Wang, L. Zhang, J. Non-Cryst. Solids 473 (2017) 79–86.
[24] B. Lu, W. Wang, Metall. Mater. Trans. B 46 (2015) 852–862.
[25] D. Xiao, W. Wang, B. Lu, Metall. Mater. Trans. B 46 (2015) 873–881.
[26] L.J. Zhou, H. Li, W.L. Wang, D. Xiao, L. Zhang, J. Yu, Metall. Mater. Trans. B 49 (2018) 2232–2240.
[27] J. Qi, C.J. Liu, M.F. Jiang, J. Non-Cryst. Solids 475 (2017) 101–107.
[28] H. Wang, P. Tang, G.H. Wen, X. Yu, Ironmak. Steelmak. 38 (2011) 369–373.
[29] L.J. Zhou, W.L. Wang, J. Wei, B.X. Lu, ISIJ Int. 53 (2013) 665–672.
[30] Z.T. Zhang, G.H. Wen, Y.Y. Zhang, Int. J. Min. Met. Mater. 18 (2011) 150–158.
[31] J. Wei, W. Wang, L. Zhou, D. Huang, H. Zhao, F. Ma, Metall. Mater. Trans. B 45 (2014) 643–652.
[32] L. Zhou, W. Wang, J. Wei, K. Zhou, ISIJ Int. 55 (2015) 821–829.
[33] J. Yang, J. Zhang, Y. Sasaki, O. Ostrovski, C. Zhang, D. Cai, Y. Kashiwaya, Metall. Mater. Trans. B 47 (2016) 2447–2458.
[34] J. Yang, J. Zhang, Y. Sasaki, O. Ostrovski, C. Zhang, D. Cai, Y. Kashiwaya, ISIJ Int. 56 (2016) 574–583.
[35] L. Zhang, W.L. Wang, S.L. Xie, K.X. Zhang, I. Sohn, J. Non-Cryst. Solids 460 (2017) 113–118.
[36] N. Takahira, M. Hanao, Y. Tsukaguchi, ISIJ Int. 53 (2013) 818–822.
[37] S.P. He, Q. Wang, D. Xie, Int. J. Min. Met. Mater. 16 (2009) 261–264.
[38] L. Wang, C. Zhang, D.X. Cai, J.Q. Zhang, Y. Sasaki, O. Ostrovski, Metall. Mater. Trans. B 48 (2017) 516–526.
[39] J.H. Park, D.J. Min, H.S. Song, ISIJ Int. 42 (2002) 344–351.
[40] H. Kim, H. Matsuura, F. Tsukihashi, W.L. Wang, D.J. Min, I. Sohn, Metall. Mater. Trans. B 44 (2013) 5–12.
[41] H. Kim, W.H. Kim, I. Sohn, D.J. Min, Steel Res. Int. 81 (2010) 261–264.
[42] A.Y. Ilyushechkin, S.S. Hla, D.G. Roberts, N.N. Kinaev, J. Non-Cryst. Solids 357 (2011) 893–902.
[43] Y. Kim, M.S. Oh, Fuel Process. Technol. 91 (2010) 853–858.
[44] Z. Wang, I. Sohn, J. Am. Ceram. Soc. 101 (2018) 4285–4296.
[45] Y.Q. Sun, J.L. Liao, K. Zheng, X.D. Wang, Z.T. Zhang, JOM 66 (2014) 2168–2175.
[46] E.I. Kamitsos, M.A. Karakassides, G.D. Chryssikos, J. Phys. Chem. 91 (1987) 1073–1079.
[47] W. Yan, W. Chen, Y. Yang, C. Lippold, A. McLean, Ironmak. Steelmak. 42 (2015) 698–704.
[48] S.F. Weng, Fourier transform infrared spectrometer, 3rd ed., Chemistry Induction Press, Beijing, 2010.
[49] R.C. Pinkerton, J. Chem. Educ. 41 (1964) 366–367.
[50] J.H. Park, D.J. Min, H.S. Song, ISIJ Int. 42 (2002) 38–43.
[51] T.S. Kim, J.H. Park, ISIJ Int. 54 (2014) 2031–2038.
[52] S. Ueda, H. Koyo, T. Ikeda, Y. Kariya, M. Maeda, ISIJ Int. 40 (2000) 739–743.
[53] G. Socrates, in: Infrared and Raman Characteristic Group Frequencies: Tables and Charts, 3rd ed., Wiley, New York, 2004.
[54] P. McMillan, B. Piriou, J. Non-Cryst. Solids 55 (1983) 221–242.
[55] V.P. Klyuev, B.Z. Pevzner, J. Non-Cryst. Solids 353 (2007) 2008–2013.